On the importance of the cracking process description for dynamic crack initiation simulation

Xi Chen, Aurélien Doitrand, Nathalie Godin, Claudio Fusco

On the importance of the cracking process description for dynamic crack initiation simulation

Xi Chen[a,*], Aurélien Doitrand[a], Nathalie Godin[a], Claudio Fusco[a]

[a]*INSA-Lyon, Universite Claude Bernard Lyon 1, CNRS, MATEIS, UMR5510, 69621, Villeurbanne, France;*

Abstract

A dynamic implementation of the coupled criterion under quasi-static loading, based only on the mean velocity during crack initiation, is proposed. It relies on a simultaneous node release method. It consists of computing the dynamic incremental energy release rate by simultaneously opening a crack of a finite length during a given time increment rather than progressively opening smaller crack increments following a velocity profile as in the progressive node release method. Both methods result in significantly different kinetic energy variations as a function of the crack length, and thus different incremental energy release rates for large enough crack velocities, for which the kinetic energy magnitude is similar to the elastic strain energy magnitude. Both simultaneous node release method and progressive node release method can however be equivalently used for small enough crack velocities since similar incremental energy release rates are obtained with both methods. Inverse identification of fracture properties based on dynamic crack initiation at a hole in Brazilian disk specimens yields critical energy release rates in the same order of magnitude as the one obtained based on dynamic crack propagation modeling.

Keywords: Dynamic coupled criterion, simultaneous node release method, progressive node release method, crack initiation, stop length

1. Introduction

Crack initiation in brittle solids under quasi-static loadings usually occurs abruptly with the sudden formation of a crack over a finite length in a short time increment [1–4]. The energy release rate (ERR) is monotonically increasing as a function of the crack length, which leads to unstable crack growth [5]. Stable crack growth after initiation may be encountered in case of non-monotonic ERR variations [6–8] for which the loading must be increased for further crack propagation. In such configurations, the crack stop length just after initiation can be measured [1, 9]. Whether stable or unstable crack growth occurs, the phenomenon of brittle crack initiation occurs ”suddenly”, i.e. during a time scale that cannot be captured by the human eye. The crack velocity, usually captured by high-speed camera or other special equipment, is generally in the order of magnitude of the Rayleigh velocity c_{R} [10–13].

*Fully documented templates are available in the elsarticle package on CTAN.

*Corresponding author
Email address: xi.chen@insa-lyon.fr (Xi Chen)

Symbol	Definition
c_{R}	Rayleigh velocity
$\mathcal{G}_{\mathrm{c}}$	Critical energy release rate
σ_{c}	Tensile strength
L, W, ϕ	Holed Brazilian Disk length, width and hole diameter
θ	Angle of the Brazilian Disk flattened part
R_1, R_2	Inner hole and outer circle radius
U	Imposed loading or displacement
U_{c}	Initiation loading level
$\dot{U}$	Prescribed displacement rate
$U_{\mathrm{i}}^{\mathrm{j}}$	Node displacement perpendicular to the direction of crack propagation
ℓ	Crack length
ℓ_{c}	Initiation crack length
$\Delta\ell$	Incremental crack length
ℓ_{stop}	Crack stop length
ℓ_{mat}	material characteristic length
$\ell_{\mathrm{stop,min}}^{\mathrm{exp}}$, $\ell_{\mathrm{stop,max}}^{\mathrm{exp}}$	Minimum and Maximum crack stop lengths measured experimentally
ℓ_{m}	Mesh size
W_{ext}	External force work
W_{el}	Elastic strain energy
W_{k}	Kinetic energy
ΔW_{ext}	Variation in the external force work
ΔW_{el}	Variation in the elastic strain energy
ΔW_{k}	Variation in the kinetic energy
$\mathcal{G}_{\mathrm{c}}\ell$	Crack surface creation energy
v_{crack}	Crack velocity
$\mathcal{G}^{\mathrm{dyn}}$	Dynamic energy release rate
$\mathcal{G}_{\mathrm{inc}}^{\mathrm{dyn}}$	Dynamic Incremental energy release rate
$A(\ell)$, $k(\ell)$	Functions depending on the problem geometry
Δt_{c}	Time interval during crack initiation
Δt	Step time
F^{R}	Reaction force
ALac	Anhydrous lactose
E, ν, ρ	Young's modulus, Poison's ratio, density

Table 1: Nomenclature of symbols used in the manuscript.

The crack velocity during crack propagation has a marked influence on the description of the crack length and direction. Sufficiently large crack velocity may lead to instabilities in the crack propagation such as oscillations [14], micro- or macro-branching [15–17]. Fast crack propagation results in inertial effects described by a non-negligible kinetic energy magnitude that can be in the same order of magnitude as elastic strain energy [18]. The ERR thus decreases with increasing crack speed because a larger fraction of the available energy is converted into kinetic energy [19–22]. If the kinetic energy is disregarded in the identification of the critical ERR, it yields a larger apparent critical energy release rate $\mathcal{G}_c$ [23–26]. Since crack initiation may occur in a short time increment, the crack velocity cannot be neglected, similar to fast crack propagation.

Linear elastic fracture mechanics (LEFM) [19, 27, 28] can assess the stable or unstable crack propagation. However, it is limited to configurations including a pre-existing crack, thus excluding crack nucleation. Crack initiation can be assessed in the framework of finite fracture mechanics (FFM) by considering finite rather than infinitesimal crack increments [29–31]. In this framework, including the theory of critical distances [32, 33], Leguillon [34] proposed the coupled criterion (CC) which requires a simultaneous fulfillment of two separate conditions, based on the stress and the incremental energy release rate (IERR) respectively. At first, the stress along the finite crack length must be larger than the tensile strength σ_c. In complement, the IERR must be larger than the critical energy release rate $\mathcal{G}_c$. The stress field and the IERR over the crack path can be obtained either through analytical functions [35, 36], matched asymptotic expansions [34, 37–40], or finite element (FE) simulations [41–44]. Up to now, most of the works focus on the quasi-static implementation of the CC and proved to be an efficient and robust approach to study crack initiation in different materials and different geometries [43, 45–48]. Only a few works are related to dynamic implementations of the CC. Laschuetza and Seelig [49] proposed to estimate the crack velocity during initiation based on a quasi-static CC approach, by ensuring that the dynamic ERR is equal to the critical ERR. Le Pavic *et al.* [50]. proposed a dependency of the material tensile and shear strengths to the loading rate to account for dynamic loadings. Another empirical approach able to account for failure load dependency on the loading rate was proposed by Chao *et al.* [51], by introducing a characteristic time over which the loading is averaged and solving the CC for the obtained average loading. An alternative dynamic implementation of the CC was finally proposed by calculating the kinetic energy in the overall energy balance [52, 53].

The latter dynamic CC approach was implemented [53] to study crack initiation in PMMA specimens with circular holes and confronted with experiments provided by Leite *et al.* [54]. The dynamic CC approach overcame the underestimation of the fracture stress predicted by the quasi-static CC approach in [54]. A major outcome of this analysis was that not only the mean initiation crack velocity but also the velocity profile during crack initiation, which had a major influence on the critical loading corresponding to crack initiation [53]. Numerical simulations thus indicate that an accurate description of the cracking process is a key point in understanding fracture. This motivation is also brought about by experimental observations of crack initiation and propagation, as a variety of fracture patterns may be encountered. It includes, e.g., stable continuous crack propagation at slow velocity [55, 56], rapid propagation near the Rayleigh wave speed [57, 58], abrupt crack nucleation [1], or alternate quasi-static and dynamic regimes (stick-slip) [59]. This raises the question of whether cracks propagate gradually or open simultaneously over a larger distance.

In this paper, we propose a dynamic CC implementation for crack initiation that relies on a simultaneous opening of the crack over a given distance and compare it to the gradual formation usually employed. In Section 2, we recall the implementation of the dynamic CC and its present extension. In Section 3, we compare two dynamic CC implementations in the case of crack initiation in a holed Brazilian disk specimen [13]. In section 4, we provide inverse identification of the tensile strength and the critical ERR based on a confrontation between the numerical simulation and experimental results.

2. Methodology

2.1. Coupled Criterion

Fig.1(a) and Fig.1(b) depict a schematic description of the geometry and loading under consideration in both uncracked and cracked specimens. L and W are the holed Brazilian Disk's length and width, respectively. The hole diameter is $\phi = 2R$. The angle θ indicates the length over which the specimen is flattened to facilitate the positioning of the sample in the testing machine [60, 61].

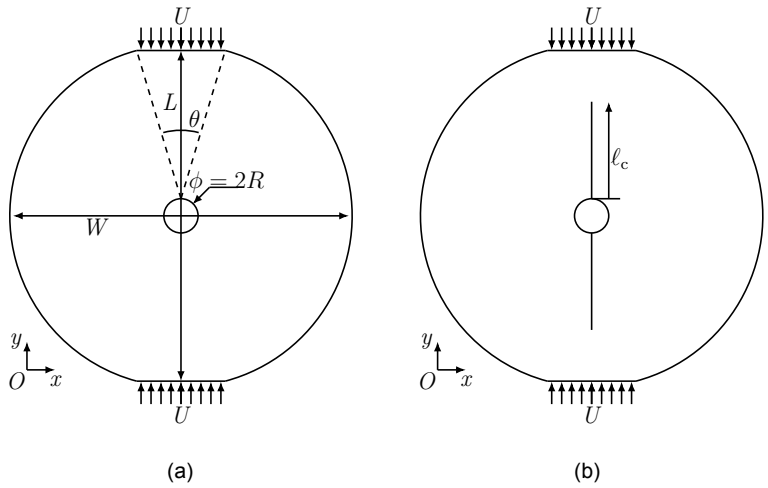

Fig. 1. Geometry and loading of the specimen (a) before crack initiation, (b) after symmetrical crack initiation.

According to the CC [34], crack initiation can only occur provided the stress and energy requirements are simultaneously fulfilled. The first CC requirement is that the stress is larger than the tensile strength σ_c across the crack path before crack initiation. This can be expressed as follows:

$$\sigma(y, U) \geqslant \sigma_c \quad \forall\, 0 \leqslant y \leqslant \ell_c, \tag{1}$$

where y is the coordinate along the crack path before initiation. U, the imposed loading or displacement, and ℓ_c, the crack initiation length, are the two problem unknowns. The second requirement is based on the principle of energy conservation between the states before and after crack initiation. In the following, the 2D CC formulation is provided for a unitary thickness. It is obtained by a balance of the variation in the external force work (W_{ext}), elastic strain energy (W_{el}), kinetic energy (W_k), and crack surface creation energy ($\mathcal{G}_c \ell$,

where $\mathcal{G}_c$ is the material fracture toughness):

$$\Delta W_{\text{ext}}(\ell, U) - \Delta W_{\text{el}}(\ell, U) - \Delta W_{\text{k}}(\ell, U) = \mathcal{G}_c \ell \tag{2}$$

Hence, finding the minimum imposed loading and crack length that meet both Equations (1) and (2) becomes the next step for solving the CC.

In the quasi-static CC approach, the incremental energy release rate (IERR) denoted $\mathcal{G}_{\text{inc}}^{\text{qs}}$ is calculated, neglecting the kinetic energy W_{k}. The dynamic CC approach is applied under quasi-static loading conditions by describing the crack length variation as a function of time instead of the assumption of an instantaneous process in the quasi-static approach. This method involves the definition of a certain velocity profile $v_{\text{crack}}(t) = \mathrm{d}\ell(t)/\mathrm{d}t$ to represent the crack length jumps from 0 to the initiation length ℓ_c in a given time. Thus, the dynamic IERR $\mathcal{G}_{\text{inc}}^{\text{dyn}}$ can be written so as to consider the kinetic energy variation due to crack initiation.

$$\mathcal{G}_{\text{inc}}^{\text{dyn}}(\ell(t), U) = \frac{\Delta W_{\text{ext}}(\ell(t), U) - \Delta W_{\text{el}}(\ell(t), U) - \Delta W_{\text{k}}(\ell(t), U)}{\ell(t)}. \tag{3}$$

Note that, for the case of prescribed displacements, $\Delta W_{\text{ext}} = 0$ and therefore, the energy balance in eq. (2) turns into the following equality:

$$\mathcal{G}_{\text{inc}}^{\text{dyn}}(\ell(t), U) = \frac{-\Delta W_{\text{el}}(\ell(t), U) - \Delta W_{\text{k}}(\ell(t), U)}{\ell(t)} = \mathcal{G}_c, \tag{4}$$

Using a linear elastic material model and small deformation assumption, for a given velocity profile, the stress is proportional to the prescribed displacement and the IERR is proportional to the square of prescribed displacement [53]:

$$\begin{cases} \mathcal{G}_{\text{inc}}^{\text{dyn}}(\ell, U) = A(\ell) U^2 = \mathcal{G}_c, \\ \sigma(\ell, U) = k(\ell) U \geqslant \sigma_c, \end{cases} \tag{5}$$

where $A(\ell)$ and $k(\ell)$ are functions depending on the problem geometry.

Based on eq. (5), the minimum loading level U_c at crack initiation and the crack initiation length ℓ_c can be determined as:

$$\begin{cases} U_c = \min\limits_{\ell} \left\{ \max\left(\sqrt{\frac{\mathcal{G}_c}{A(\ell)}}, \frac{\sigma_c}{k(\ell)} \right) \right\}, \\ \ell_c = \operatorname{argmin}\limits_{\ell} \left\{ \max\left(\sqrt{\frac{\mathcal{G}_c}{A(\ell)}}, \frac{\sigma_c}{k(\ell)} \right) \right\}, \end{cases} \tag{6}$$

Functions $A(\ell)$ and $k(\ell)$ can be obtained for any imposed displacement, exploiting the proportionality between the stress (resp. energy) and the prescribed displacement (resp. square prescribed displacement). For a given velocity profile and material density, the crack initiation length and the initiation displacement are obtained using eq. (6) for any $(\sigma_c, \mathcal{G}_c)$ couples. More details about the FE implementation of the CC dynamic approach are given in [52, 53].

2.2. Crack propagation

Once the crack initiation length ℓ_c and the critical loading U_c are determined by the dynamic CC approach, the crack growth can be studied based on the ERR, which can be computed from $\mathcal{G}_{\text{inc}}^{\text{dyn}}$ [62]:

$$\mathcal{G}^{\text{dyn}}(U, \ell(t)) = -\frac{\mathrm{d}W_{\text{el}}(U, \ell(t))}{\mathrm{d}\ell} - \frac{\mathrm{d}W_{\text{k}}(U, \ell(t))}{\mathrm{d}\ell} = \frac{\mathrm{d}\mathcal{G}_{\text{inc}}^{\text{dyn}}(U, \ell(t))}{\mathrm{d}\ell} \ell + \mathcal{G}_{\text{inc}}^{\text{dyn}}(U, \ell(t)), \tag{7}$$

After crack initiation, the crack propagates in a stable or unstable manner until $\mathcal{G}^{\mathrm{dyn}} < \mathcal{G}_{\mathrm{c}}$. For stable crack propagation, an increasing loading is necessary to make the crack grow, whereas, unstable propagation corresponds to a crack growth without any increase in the loading up to a certain stop length for which $\mathcal{G}^{\mathrm{dyn}} \leqslant \mathcal{G}_{\mathrm{c}}$. In the particular case where the initiation length corresponds to the length maximizing $\mathcal{G}^{\mathrm{dyn}}_{\mathrm{inc}}$, the stop length is equal to the initiation length [62].

Crack initiation occurs at an imposed displacement U_{c}, over a length ℓ_{c} and during a time Δt_{c}. As a consequence, there is a slight increase in the imposed displacement during the time interval Δt_{c} so that after initiation, the imposed displacement is actually $U_{\mathrm{c}} + \Delta t_{\mathrm{c}} \times \dot{U}$, where $\dot{U}$ is the prescribed displacement rate.

To account for the displacement increase during initiation, the stop length is calculated based on the condition: $\mathcal{G}^{\mathrm{dyn}}(\ell(t), U_{\mathrm{c}} + \dot{U}\Delta t_{\mathrm{c}}) = \mathcal{G}_{\mathrm{c}}$.

2.3. Node Release Method

Implementing the energy criterion requires the calculation of the IERR as a function of the crack length for a given crack velocity profile, which was previously done using a progressive node release method (PNRM) [52, 53], recalled in Section 2.3.1. Another approach to obtain the IERR based only on the mean crack velocity during initiation, the simultaneous node release method (SNRM), is presented in Section 2.3.2. First, it can be noted that for both PNRM and SNRM, Dirichlet boundary conditions are first prescribed for all the nodes lying over the crack path to represent the configuration without crack and calculate the stress condition of the CC. The stress condition is thus the same whatever the node release method.

2.3.1. Progressive Node Release Method

For the progressive node release method, the IERR is calculated by progressively releasing the Dirichlet boundary condition of each of these nodes, following a prescribed velocity profile, as shown in Fig.2(a). The horizontal axis and the vertical axis represent the time duration and the crack length respectively. The figure's top partition shows the node release process from the initial state without crack. Initially, the two crack lips are free surfaces. The first crack lip is thus represented by a set of nodes and for each node of this set, there exists a node of the second crack lip node set that geometrically lies in the exact same position but belongs to another element. Before the node release, we impose that the displacement of each pair of corresponding nodes from the two crack lips must be the same, which induces a reaction force F^{R} that maintains both nodes at the same position. Starting from this initial state, the stress condition is obtained for all nodes over the crack length. Then, the node release is obtained by canceling the equality condition of both node degrees of freedom. Actually, we adopt a linear reaction force decrease during the release of one node pair to ensure energy dissipation due to crack propagation. At the end of the node release step, the displacement jump ΔU represents the distance between the two nodes free of any interaction. One node is released in one step to simulate an incremental crack length $\Delta\ell$ between two consecutive crack lengths ($\Delta\ell = \ell_{\mathrm{i}+1} - \ell_{\mathrm{i}}$). $U^{\mathrm{j}}_{\mathrm{i}}$ is the node displacement perpendicular to the direction of crack propagation. i and j correspond to the node number (0, 1, 2...) and the crack length number (ℓ_1, ℓ_2, and ℓ_3...). After releasing all nodes along the crack path, the elastic strain energy and the kinetic energy as a function of the crack length are obtained so that the IERR

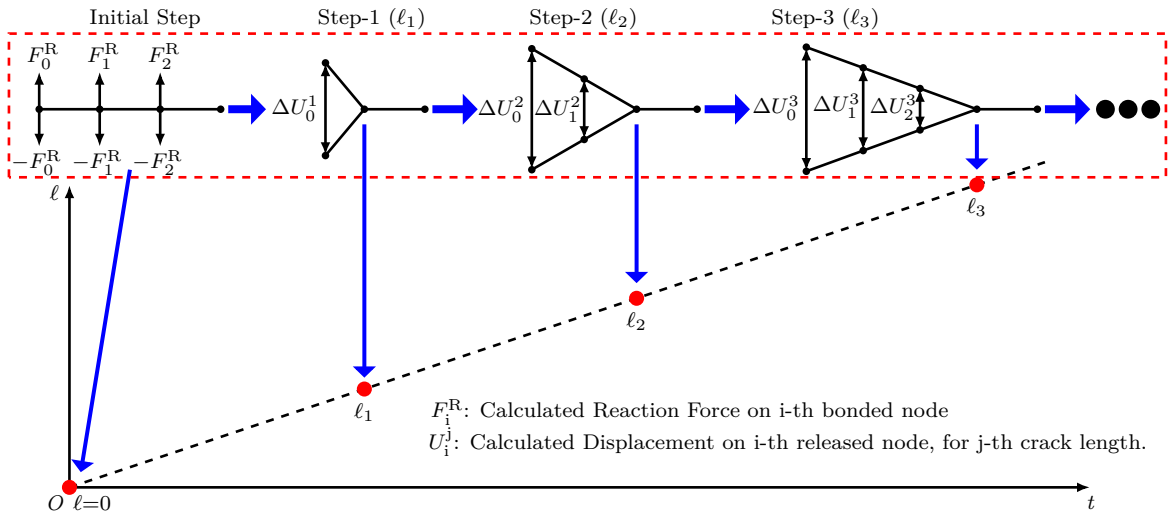

(a)

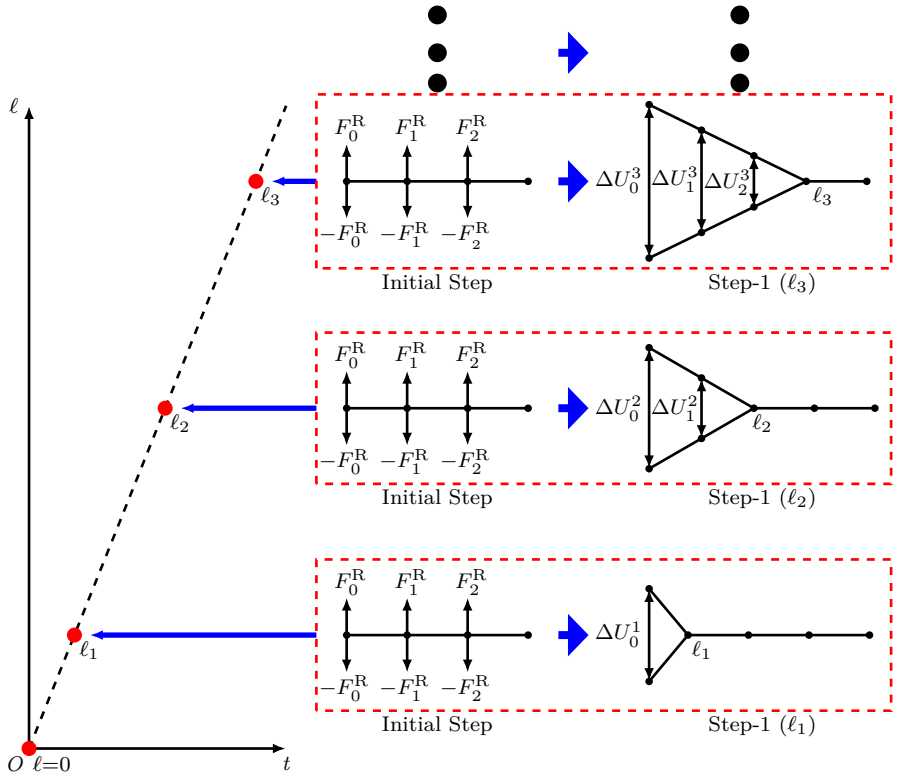

(b)

Fig. 2. Variation of the crack length as a function of time and corresponding crack configuration for (a) progressive node release method; (b) simultaneous node release method. One red dashed rectangular corresponds to one FE calculation.

can be computed by eq. 4. The step time of each step Δt can be determined by the crack velocity and the incremental crack length as $\Delta t = \Delta\ell / v_{\mathrm{crack}}$, assuming a constant crack velocity during crack initiation. For each node release step, 10 iterations are used.

2.3.2. Simultaneous Node Release Method

The simultaneous node release method (SNRM) consists in calculating the IERR for a given crack length ℓ by simultaneously releasing the Dirichlet boundary conditions of all the nodes lying over the given crack length in a step time Δt so that the crack velocity is $v_{\mathrm{crack}} = \ell / \Delta t$. It thus gets rid of the requirement of a crack velocity profile, but only requires a mean velocity during initiation as input. Contrary to the PNRM which can be implemented in a single FE calculation, one FE calculation is required for each crack length, as shown in Fig.2(b). The IERR can be computed as a function of the crack length using eq. 4, based on the elastic strain energy W_{el} and the kinetic energy W_{k} obtained for each crack length. For each step, 10 iterations are used.

3. Numerical Implementation

3.1. Configuration under Investigation

The failure of the holed Brazilian Disk specimen under compression is studied in order to compare the PNRM and the SNRM. Because of the geometry and loading symmetry, only a quarter of the Brazilian Disk is modeled, as indicated in Fig.3. The length and the width of the quarter-holed Brazilian Disk are 8 mm and 7.7 mm, respectively. The specimen thickness is 3.5 mm. The hole radius R_1 is 0.25 mm and the radius of the outer circle R_2 is 8 mm. The length of the upper flattened edge is 0.78 mm (the angle of the flattened part is 30°). All nodes of the upper edge are subjected to a displacement U along the y direction, while the left and bottom edges are subjected to symmetry conditions. The symmetry condition on the crack path (over a distance) is then released based on the chosen node release method in order to calculate the ERR and IERR. To capture accurately the variation of the energy, a mesh consisting of 4-node linear plain strain 2D elements is used. The mesh is refined along the hole edge with uniform mesh size ℓ_{m} =0.02 mm. A finer mesh size results in differences smaller than 2% on the IERR and stress functions. The material under investigation is anhydrous lactose (ALac) and the material properties determined in [13] are given in Table 2.

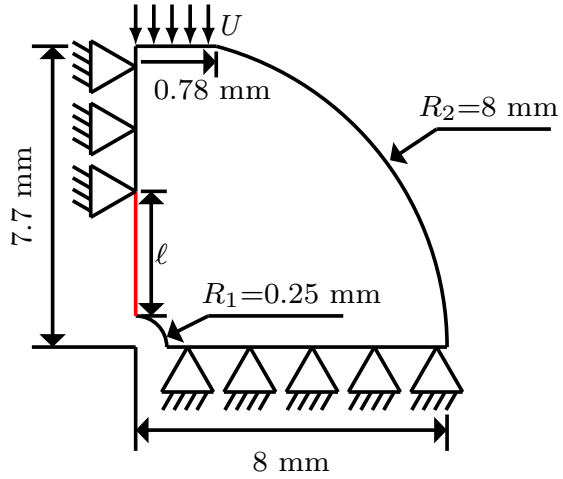

Fig. 3. Finite element model geometry of the Brazilian disk specimen.

E (MPa)	ν	ρ (kg/m^3)	σ_c (MPa)	$G_c(\mathrm{J/m^2})$
8400	0.24	1347	2.3 - 2.6	1.9

Table 2: Young's modulus (*E*), Poisson's ratio (ν), density (ρ) , tensile strength and critical ERR of ALac [13, 63]

3.2. Experimental Input Data

Croquelois *et al.* [13] studied dynamic crack propagation in ALac by performing compression experiments on holed Brazilian Disk specimens. Six Brazilian Disks with a circular hole (diameter ϕ = 0.5 mm) underwent compression tests to examine the crack initiation and propagation from the hole. The measured crack initiation force was 278 $\pm$ 2 N. A high-speed camera recorded the crack tip locations during the dynamic crack propagation. The crack tip position exhibited a linear variation as a function of time with an average crack velocity ranging from 0.45c_R to 0.7c_R, where $c_\mathrm{R} \simeq 1452\ \mathrm{m/s}$ is the Rayleigh velocity. After dynamic propagation, the measured crack extension ranged from 3.8 $\pm$ 0.25 mm and 5.9 $\pm$ 0.25 mm to lie between 3.6 mm to 6.2 mm. Then, a linear relationship between the crack length and the time duration was observed, the propagation time ranging from $4.3\,\mu\mathrm{s}$ to $8.6\,\mu\mathrm{s}$. Based on finite element modeling of the dynamic crack propagation at 0.45c_R crack velocity, the material critical ERR was determined as 1.9 $\mathrm{J/m^2}$ (note that a value of 6 $\mathrm{J/m^2}$ was obtained if the inertial effect due to dynamic propagation was neglected).

4. Comparison between PNRM and SNRM

We evaluate the ability of the PNRM and SNRM to model crack initiation from a circular hole in a holed Brazilian Disk specimen under compression loading. Dirichlet boundary conditions are prescribed at the specimen's flat edge so as to obtain the initiation force measured experimentally [13].

4.1. Energy and IERR variations

The variation of elastic strain energy ($-\Delta W_{\mathrm{el}}$) and kinetic energy (ΔW_{k}) as a function of the crack length using PNRM and SNRM are shown in Fig.4(a) and Fig.4(b) for v_{crack} = 0.1c_{R}, and in Fig.4(c) and Fig.4(d) for v_{crack} = 0.7c_{R}. For the smaller crack velocity, the elastic strain energy variation is similar whatever the crack length for both node release methods (Fig.4(a)) whereas for the larger crack velocity, the node release method induces difference for sufficiently large crack lengths (Fig.4(c)). Different kinetic energy variations are obtained for sufficiently large crack lengths using either PNRM or SNRM whatever the crack velocity (Fig.4(b) and Fig.4(d)). However, for a given crack length, for v_{crack} = 0.1c_{R}, the magnitude of ΔW_{k} is 10 times smaller than the magnitude of $-\Delta W_{\mathrm{el}}$. Thus, the variation of kinetic energy has no influence on the IERR. For v_{crack} = 0.7c_{R}, $-\Delta W_{\mathrm{el}}$ and ΔW_{k} are in the same order of magnitude for a given crack length so that the difference of kinetic energy induced by the node release method has a larger influence on the IERR, especially for large enough cracks.

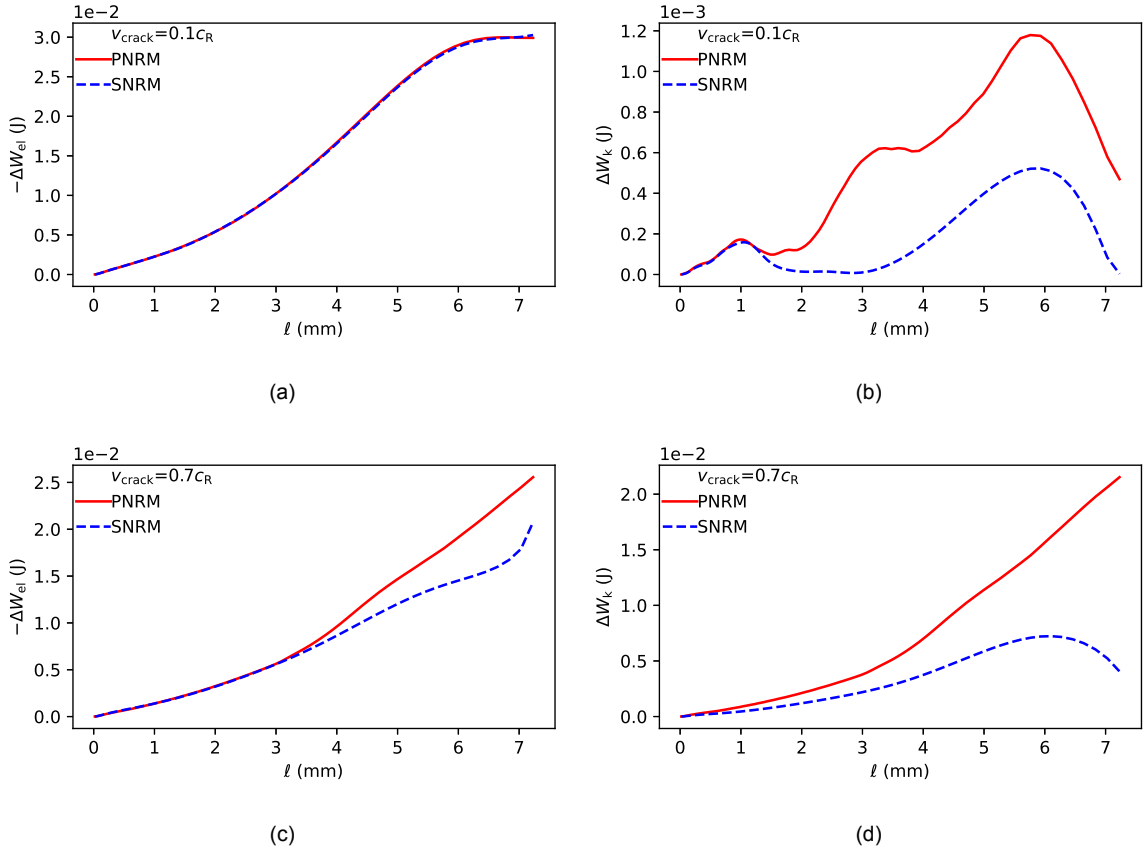

Fig. 4. Variation of (a and c) elastic strain energy ($-\Delta W_{\mathrm{el}}$) and (b and d) kinetic energy (ΔW_{k}) as a function of the crack length ℓ using PNRM and SNRM. (a and b) v_{crack} = 0.1c_{R}; (c and d) v_{crack} = 0.7c_{R}.

Fig.5 shows the dynamic IERR as a function of the crack length for different crack velocities (from 0.1c_{R}, to 0.7c_{R}). Whatever the node release method, the larger the crack velocity, the smaller the dynamic IERR. For all crack velocities, the dynamic IERR shows an overall increasing trend up to a maximum value, corresponding to a crack length of about 5 to 6 mm. A secondary local maximum with a smaller magnitude is also attained

for a crack length smaller than 1 mm. A similar variation of the dynamic ERR is obtained for SNRM in Fig.5(b). except for sufficiently large crack velocity, for which the dynamic IERR also increases for large crack lengths (Fig.5(b)).

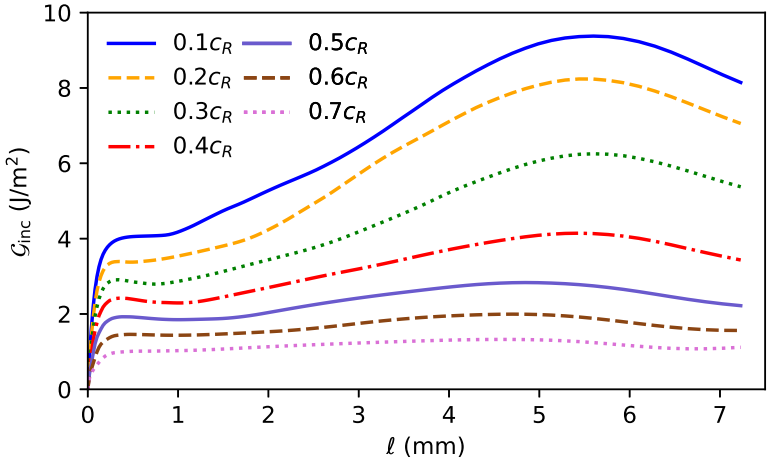

(a)

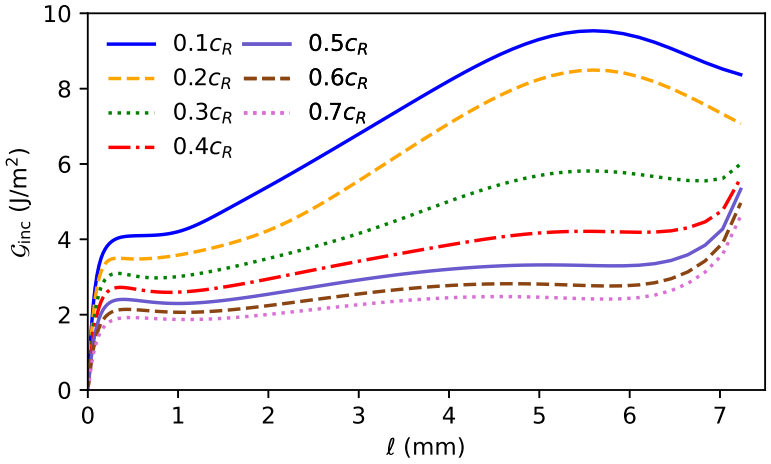

(b)

Fig. 5. Dynamic IERR as a function of crack length ℓ for different crack velocities using (a) PNRM, and (b) SNRM.

Fig.6 shows the IERR and the ERR as a function of the crack length using different node release methods for a small crack velocity (v_{crack} = 0.1c_{R}), as shown in Fig.6(a) and Fig.6(b), and a large crack velocity (v_{crack} = 0.7c_{R}), as shown in Fig.6(c) and Fig.6(d). It is found that for 0.1c_{R} crack velocity, the results for IERR and ERR using either PRNM or SNRM are similar. However, for the larger crack velocity, the ERR and the IERR using the SNRM are larger than that using the PNRM. This is mainly due to the kinetic energy contribution, that is significantly smaller for the SNRM than for the PNRM whereas the elastic strain energy contribution is closer for both methods. The kinetic energy thus strongly depends on the cracking process.

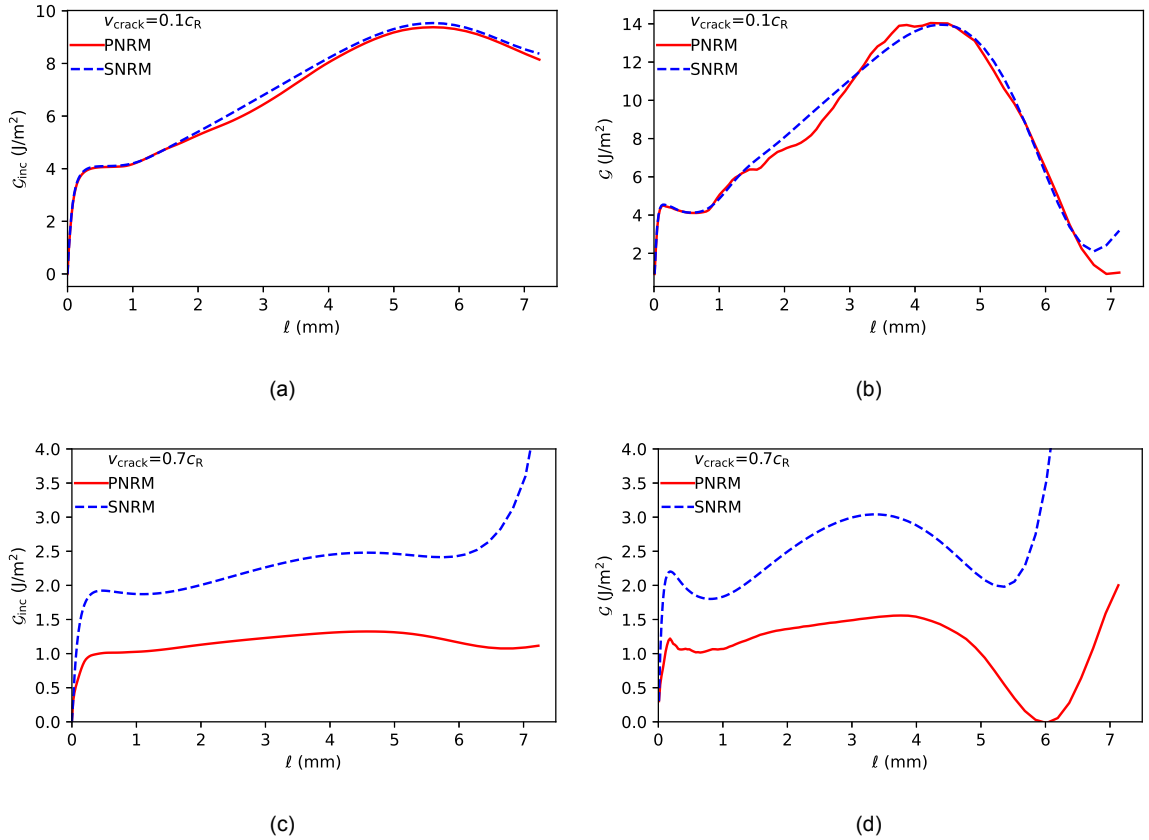

Fig. 6. IERR and ERR as a function of the crack length using the PNRM and the SNRM for different crack velocities: (**a**) and (**b**) for v_{crack} = 0.1c_{R} and (**c**) and (**d**) for v_{crack} = 0.7c_{R}.

4.2. Dynamic Coupled Criterion Solution

When solving the CC, several configurations may be encountered depending on the (σ_{c}, $\mathcal{G}_{\mathrm{c}}$) values. Three main cases can be distinguished, which are represented in Fig.7, the red dot indicating the initiation crack length ℓ_{c}. In Fig.7(a) and Fig.7(c), the right figure is a zoom of the region around the initiation crack length ℓ_{c}. **Case 1**: For large σ_{c} and small $\mathcal{G}_{\mathrm{c}}$, a small crack initiation length is obtained (ℓ_{c} < 1 mm), and the initiation loading depends on both stress and energy criteria, as shown in Fig.7(a). **Case 2**: For small σ_{c} and large $\mathcal{G}_{\mathrm{c}}$, a larger crack initiation length from 1.6 mm to 4 mm is obtained, as shown in Fig.7(b) and the initiation loading is also dependent on both stress and energy criteria. **Case 3**: The third case arises for intermediate σ_{c} and $\mathcal{G}_{\mathrm{c}}$ values, for which crack initiation is controlled by the energy criterion, as shown in Fig.7(c). The initiation length corresponds to the length maximizing $\mathcal{G}_{\mathrm{inc}}$ and the stress criterion is fulfilled for a larger crack length ($\ell \geq \ell_{\mathrm{c}}$). This case arises in the presence of the local IERR maximum equal to $\mathcal{G}_{\mathrm{c}}$ for small crack lengths.

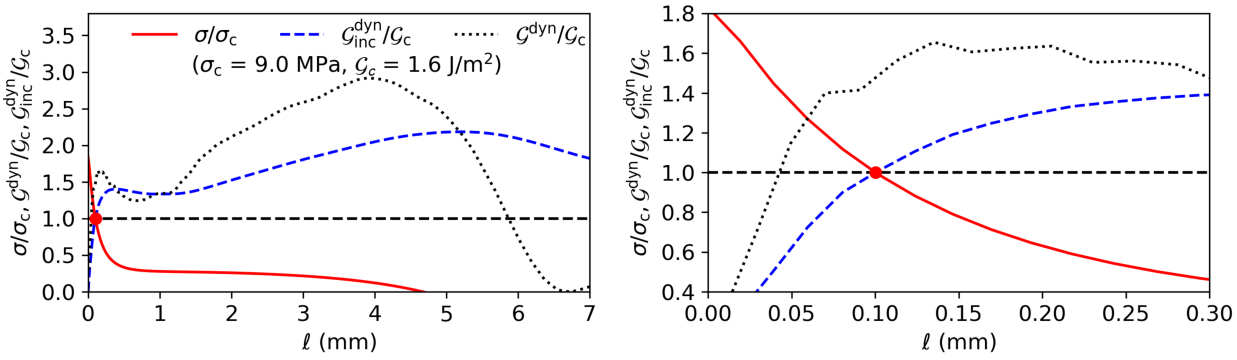

(a)

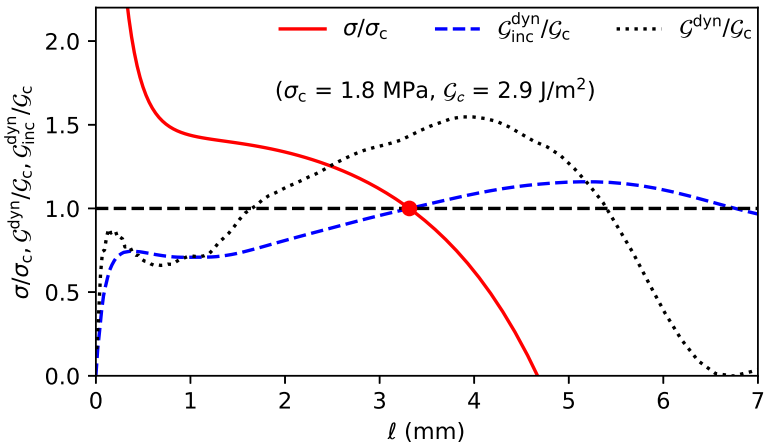

(b)

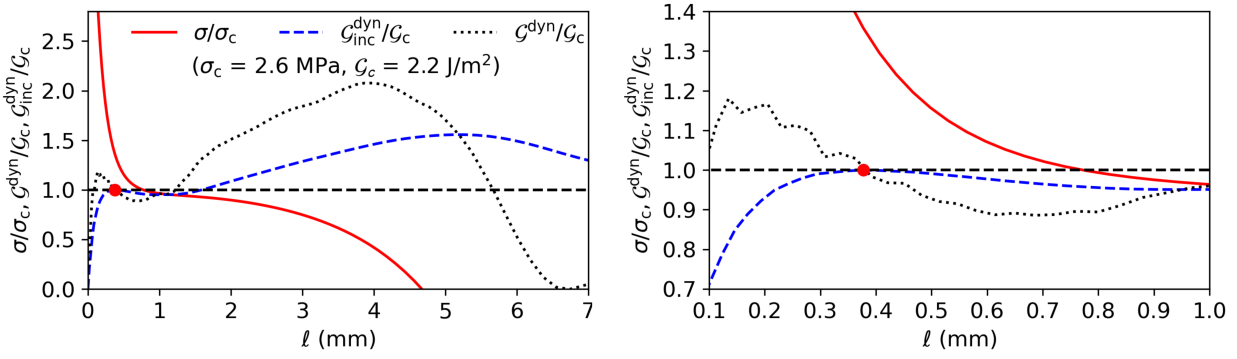

(c)

Fig. 7. Stress, IERR, and ERR as a function of the crack length for different (σ_c and $\mathcal{G}_c$): **(a)** σ_c = 9.0 MPa, $\mathcal{G}_c$ = 1.6 J/m^2; **(b)** σ_c = 1.8 MPa, $\mathcal{G}_c$ = 2.9 J/m^2; **(c)** σ_c = 2.6 MPa, $\mathcal{G}_c$ = 2.2 J/m^2.

4.3. *Fracture parameter identification based on initiation force*

The solution of the CC dynamic approach enables us to determine for a given (σ_c, $\mathcal{G}_c$) couple, the crack initiation length as well as the initiation displacement or remote force (Equation 6). Since the initiation force has been measured experimentally, it is thus possible to determine, for a given crack velocity and node release method, all (σ_c, $\mathcal{G}_c$) couples for which the experimental initiation force is retrieved. Fig.8 shows admissible (σ_c, $\mathcal{G}_c$) couples, identified using the dynamic CC approach to retrieve the experimental initiation force, for different crack velocities (v_{crack} = 0.45c_{R} or v_{crack} = 0.7c_{R}) and different node release methods. Fig.8(a) shows the results for v_{crack} = 0.45c_{R} using the PNRM. It is observed the critical ERR decreases with increasing tensile strength. Overall, the three cases described in Section 4.2 are retrieved. **Case 1**: For σ_c > 3.5 MPa, the case presented in Fig.7(a) is encountered, which corresponds to initiation lengths so that the IERR is smaller than the local maximum value, indicated by the black upward pointing triangles. **Case 2**: For σ_c < 2.8 MPa, the case, indicated by the orange downward pointing triangles, corresponding to the configuration is presented in Fig.7(b). We retrieve a decreasing critical ERR with increasing tensile strength since both energy and stress conditions drive the initiation loading. **Case 3**: For configurations corresponding to Fig.7(c), a constant critical ERR is obtained since the initiation loading solely depends on the energy criterion, indicated by the blue circles. Depending on the crack velocity and the chosen node release method, either two or three configurations are encountered, the latter situation occurring provided the presence of the local maximum for sufficiently small crack lengths. The difference in the critical ERR obtained using both methods is not larger than 0.3 $\mathrm{J/m^2}$ for crack velocity v_{crack} = 0.45c_{R}. For a large crack velocity v_{crack} = 0.7c_{R}, the critical ERR obtained using the SNRM is significantly larger than that using the PNRM for a fixed value of σ_c. Differences up to 1.2 $\mathrm{J/m^2}$ are obtained depending on the chosen node release method.

Based solely on the initiation force The dynamic approach of the CC enables the determination of all admissible ($\sigma_c, \mathcal{G}_c$) couples for a given crack velocity and node release method. These couples are relatively similar for both node release methods for sufficiently low crack velocities and significantly differ for large crack velocities.

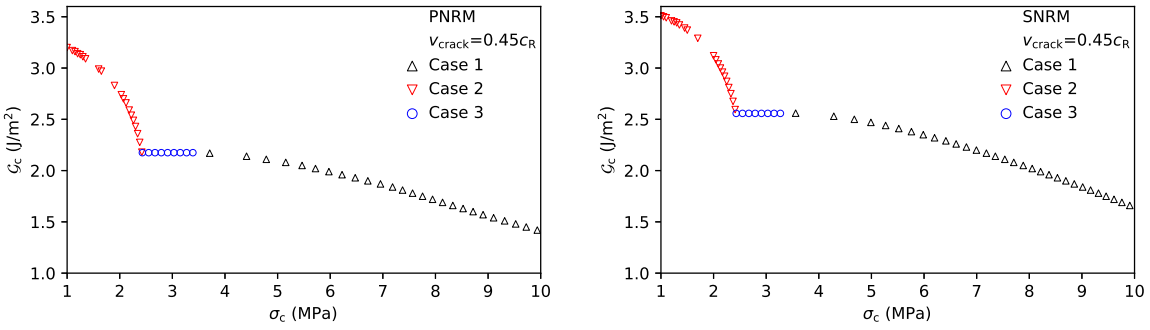

(a) (b)

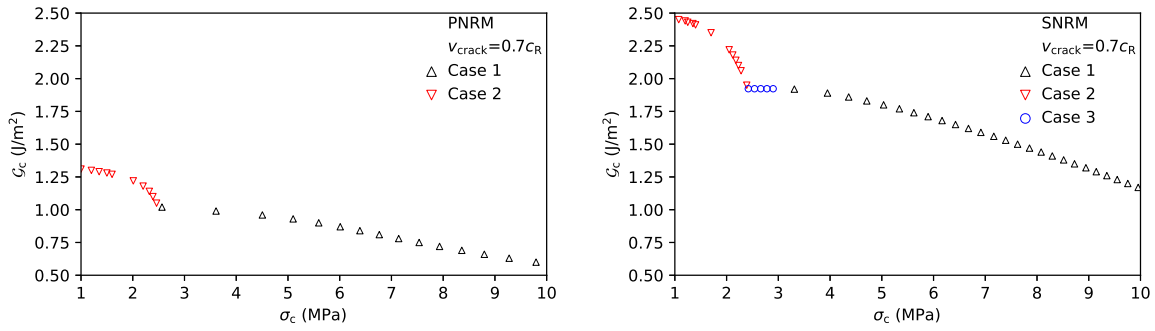

(c) (d)

Fig. 8. Admissible $(\sigma_c, \mathcal{G}_c)$ couples for which the experimentally measured initiation force is retrieved using the dynamic CC approach. (**a** and **b**): v_{crack} = 0.45c_R; (**c** and **d**): v_{crack} = 0.7c_R. (**a** and **c**): using the PNRM and (**b** and **d**): using the SNRM.

4.4. Fracture parameter identification based on crack stop length

In addition to the initiation force, the experiments provide the measurement of the crack stop length after unstable propagation following crack initiation. It is also possible to estimate the crack stop length based on the provided modeling, so as to narrow the estimated range of admissible $(\sigma_c, \mathcal{G}_c)$ couples. The stop length ℓ_{stop} is predicted by linear elastic fracture mechanics so that $\mathcal{G}^{\text{dyn}}(\ell_{\text{stop}}) = \mathcal{G}_c$ and $\frac{\mathrm{d}\mathcal{G}^{\text{dyn}}}{\mathrm{d}\ell}(\ell_{\text{stop}}) < 0$. We recall that the stop lengths measured experimentally lie between 3.6 mm and 6.2 mm (See Section 3.2).

Fig.9(a) shows the crack initiation length, indicated by the circle, and the stop length, indicated by the triangle as a function of the material characteristic length ℓ_{mat} for v_{crack} = 0.45c_R. The material characteristic length is a dimensionless parameter expressed as $\ell_{\text{mat}} = \frac{E\mathcal{G}_c}{(1-\nu^2)\sigma_c^2}$. The crack initiation length increases with increasing material characteristic lengths, except for the constant length value that is solely determined by the energy requirement. $\ell^{\text{exp}}_{\text{stop,min}}$ and $\ell^{\text{exp}}_{\text{stop,max}}$ are the experimental results measured in [13]. For v_{crack} = 0.45c_R, compared with the experimental results, all data points in Case 1 and some data points in Case 3 are in the experimental range, and the corresponding $(\sigma_c, \mathcal{G}_c)$ couples allow retrieving the experimentally measured crack stop lengths. All $(\sigma_c, \mathcal{G}_c)$ couples in Case 3 can not be admissible because they do not match the actual observations of the stop length made in the experiment. The same operation is undergone for the other two crack velocities (v_{crack} = 0.6c_R and v_{crack} = 0.7c_R), as shown in Fig.9(b) and Fig.9(c). It is found that for these two crack velocities, all stop lengths are in the experimental range so that all predicted $(\sigma_c, \mathcal{G}_c)$ are accepted according to the comparison of the stop length.

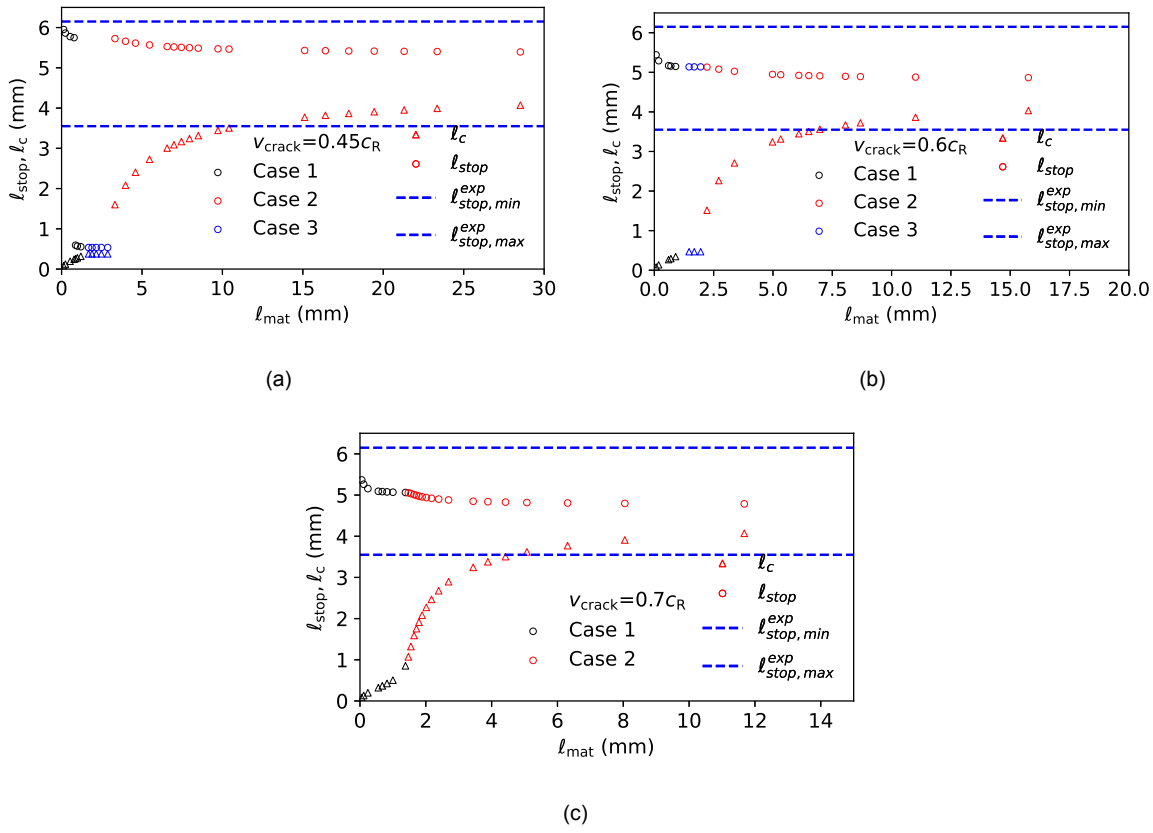

Fig. 9. Stop length for **(a)** v_{crack} = 0.45c_{R}, **(b)** v_{crack} = 0.6c_{R}, and **(c)** v_{crack} = 0.7c_{R}, using the PNRM. Different colors indicate different cases as presented in Fig.7. The upward pointing triangles indicate the initiation length and the circle indicates the stop length. Two blue dotted lines indicate the experimentally measured stop length range in [13].

Fig.10(a) summarizes the $(\sigma_{\mathrm{c}}, \mathcal{G}_{\mathrm{c}})$ couples which allow retrieving both the initiation force and the stop length corresponding to the experimental results for v_{crack} = 0.45c_{R}, 0.6c_{R}, 0.7c_{R} using the PNRM. In this figure, two dotted lines show the fracture strength range of the used material in [63], from 2.3 to 2.6 MPa. Among this range, it is possible to estimate $\mathcal{G}_{\mathrm{c}}$, as shown in Fig.10(b). It shows that the estimated $\mathcal{G}_{\mathrm{c}}$ for three crack velocities (0.45c_{R}, 0.6c_{R}, and 0.7c_{R}) and also shows the estimated value (1.9 $\mathrm{J/m^2}$) obtained by modeling of dynamic crack propagation [63], for v_{crack} = 0.45c_{R}. It is found that the larger the crack velocity, the smaller the estimated $\mathcal{G}_{\mathrm{c}}$. The estimated critical ERR for 0.45c_{R}, ranges from 2.2 $\mathrm{J/m^2}$ to 2.4 $\mathrm{J/m^2}$, which is in the same order of magnitude as the critical ERR estimated by Croquelois [63] based on the study of the unstable crack propagation phase only.

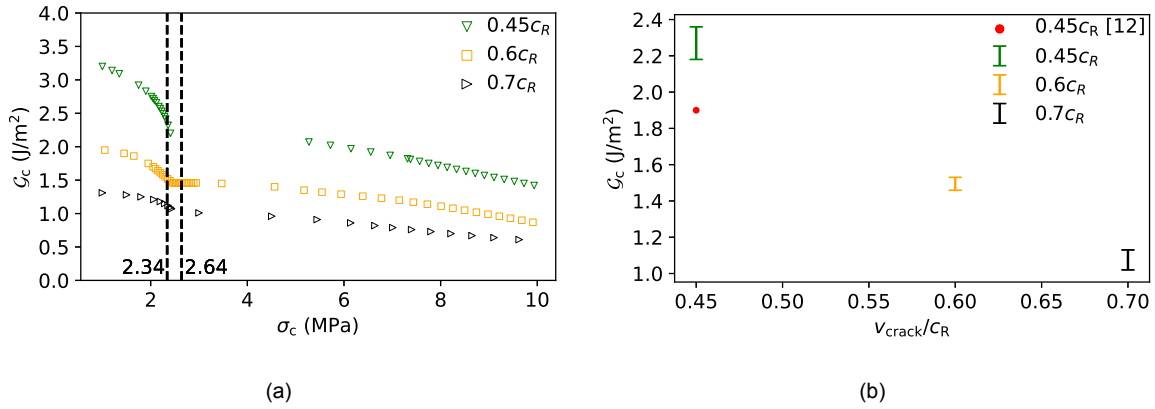

(a) (b)

Fig. 10. (a) $(\sigma_c, \mathcal{G}_c)$ couples which allow retrieving both the initiation force and the stop length corresponding to the experimental results using the PNRM: two dotted lines show the fracture strength range of the used material in [63]; (b) The estimated $\mathcal{G}_c$, and the red circle indicates the estimated critical ERR in [13] by only simulation of the dynamic crack propagation. Three crack velocities ($0.45c_R$, $0.6c_R$, and $0.7c_R$) are used.

5. Conclusion

Modeling dynamic crack initiation based on a simultaneous node release method only requires a mean crack velocity during initiation, contrary to a progressive node release method for which a velocity profile must be provided.

The SNRM induces a main difference in the kinetic energy variation as a function of the crack length compared to the PNRM. It results in similar IERR using both methods for low crack velocities, for which the kinetic energy variation magnitude remains smaller than the elastic strain energy variation magnitude. Significant differences in the IERR are obtained for larger crack velocities, the IERR being larger using the SNRM than using the PNRM.

The application of the dynamic CC approach to retrieve the initiation force measured experimentally in holed Brazilian disk specimens enables us to determine a range of admissible $(\sigma_c, \mathcal{G}_c)$ couples, which is further narrowed by comparing the crack stop length after unstable propagation following initiation. The critical ERR values identified based on dynamic crack initiation modeling ranges in the same order of magnitude as those previously determined based on unstable crack propagation modeling [13].

Here, a constant velocity profile during the crack initiation is assumed when using the PNRM. Future work will cover studying various velocity profiles using the SNRM to evaluate whether its influence on crack initiation description is as marked as in the PNRM [52, 53].

References

[1] A. Doitrand, R. Estevez, D. Leguillon, Experimental characterization and numerical modeling of crack initiation in rhombus hole pmma specimens under compression, European Journal of Mechanics - A/Solids 76 (2019) 290–299. doi:10.1016/j.euromechsol.2019.04.013.

[2] M. Funk, J. Bär, Influence of crack initiation on short crack propagation and cyclic lifetime of AA 7475-t761, Procedia Structural Integrity 13 (2018) 279–284. doi:10.1016/j.prostr.2018.12.047.

[3] K. Ravi-Chandar, W. G. Knauss, An experimental investigation into dynamic fracture: I. crack initiation and arrest, International Journal of Fracture 25 (4) (1984) 247–262. doi:10.1007/BF00963460.

[4] P. J. Singh, S. Amaldhasan, V. Chaswal, S. Aravindan, Creep crack initiation and growth in aisi 316 (n) weld – fem and experiments, Materials at High Temperaturesdoi:10.1179/096034007X207606.

[5] A. Doitrand, D. Leguillon, 3D application of the coupled criterion to crack initiation prediction in epoxy/aluminum specimens under four point bending, International Journal of Solids and Structures 143 (2018) 175–182. doi:10.1016/j.ijsolstr.2018.03.005.

[6] A. Sapora, P. Cornetti, Crack onset and propagation stability from a circular hole under biaxial loading, International Journal of Fracture 214 (2018) 97–104. doi:10.1007/s10704-018-0315-6.

[7] A. Doitrand, C. Fagiano, N. Carrère, V. Chiaruttini, M. Hirsekorn, Damage onset modeling in woven composites based on a coupled stress and energy criterion, Engineering Fracture Mechanics 169 (2017) 189–200. doi:10.1016/j.engfracmech.2016.11.021.

[8] E. Martin, D. Leguillon, Energetic conditions for interfacial failure in the vicinity of a matrix crack in brittle matrix composites, International Journal of Solids and Structures 41 (2004) 6937–6948. doi:10.1016/j.ijsolstr.2004.05.044.

[9] P. Weißgraeber, S. Hell, W. Becker, Crack nucleation in negative geometries 168 (2016) 93–104. doi:10.1016/j.engfracmech.2016.02.045.

[10] A. Petit, S. Pokam, F. Mazen, S. Tardif, D. Landru, O. Kononchuk, N. B. Mohamed, M. P. Olbinado, A. Rack, F. Rieutord, Brittle fracture studied by ultra-high speed synchrotron x-ray diffraction imaging (arXiv:2204.05683), arXiv:2204.05683 [cond-mat, physics:physics]. doi:10.48550/arXiv.2204.05683.

[11] E. Bouchbinder, T. Goldman, J. Fineberg, The dynamics of rapid fracture: instabilities, nonlinearities and length scales, Reports on Progress in Physics 77 (4) (2014) 046501. doi:10.1088/0034-4885/77/4/046501.

[12] Z. Y. Zhang, Z. Duan, F. H. Zhou, Velocity-toughening and crack speed oscillations in the dynamic fracture of pmma plates, Applied Mechanics and Materials 566 (2014) 298–304. doi:10.4028/www.scientific.net/AMM.566.298.

[13] B. Croquelois, J. B. Kopp, J. Girardot, P. Tchoreloff, V. Mazel, Dynamic fracture analysis in Brazilian test: application to pharmaceutical tablets, International Journal of Fracture 229 (1) (2021) 113–124. doi:10.1007/s10704-021-00544-9.

[14] J. Fineberg, S. P. Gross, M. Marder, H. L. Swinney, Instability in the propagation of fast cracks, Physical Review B 45 (10) (1992) 5146–5154. doi:10.1103/PhysRevB.45.5146.

[15] E. Sharon, S. P. Gross, J. Fineberg, Local crack branching as a mechanism for instability in dynamic fracture, Physical Review Letters 74 (25) (1995) 5096–5099. doi:10.1103/PhysRevLett.74.5096.

[16] E. Sharon, J. Fineberg, Microbranching instability and the dynamic fracture of brittle materials, Physical Review B 54 (10) (1996) 7128–7139. doi:10.1103/PhysRevB.54.7128.

[17] J. Fineberg, The Dynamics of Rapidly Moving Tensile Cracks in Brittle Amorphous Material, world scientific, 2006, p. 104–146. doi:10.1142/9789812773326_0003.

[18] T. Corre, M. Coret, E. Verron, B. Leble, F. Lay, Experimental full field analysis for dynamic fracture of elastomer membranes, International Journal of Fracture 223. doi:10.1007/s10704-020-00447-1.

[19] L. B. Freund, Dynamic fracture mechanics, Cambridge monographs on mechanics and applied mathematics, Cambridge University Press, Cambridge; New York, 1990.

[20] A. Coré, J.-B. Kopp, J. Girardot, P. Viot, Dynamic energy release rate evaluation of rapid crack propagation in discrete element analysis, International Journal of Fracture 214 (1) (2018) 17–28. doi:10.1007/s10704-018-0314-7.

[21] E. Sharon, J. Fineberg, Conforming the continuum theory of dynamic brittle fracture for fast cracks 397.

[22] J.-B. Kopp, C. Fond, G. Hochstetter, Rapid crack propagation in pa11: An application to pipe structure, Engineering Fracture Mechanics 202 (2018) 445–457. doi:10.1016/j.engfracmech.2018.08.025.

[23] D. J. Macon, G. L. Anderson, Kinetic energy corrections for slip-stick behavior in brittle adhesives, Journal of Applied Polymer Science 86 (8) (2002) 1821–1828. doi:10.1002/app.11090.

[24] J. W. Dally, W. L. Fourney, G. R. Irwin, On the uniqueness of the stress intensity factor? crack velocity relationship, International Journal of Fracture 27 (3–4) (1985) 159–168. doi:10.1007/BF00017965.

[25] A. J. Rosakis, A. T. Zehnder, On the dynamic fracture of structural metals, International Journal of Fracture 27 (3–4) (1985) 169–186. doi:10.1007/BF00017966.

[26] K. Ravi-Chandar, W. Knauss, Processes controlling fast fracture of brittle solids, Computing in Science Engineering 1 (5) (1999) 24–31. doi:10.1109/5992.790584.

[27] A. A. Griffith, G. I. Taylor, Vi. the phenomena of rupture and flow in solids, Philosophical Transactions of the Royal Society of London. Series A, Containing Papers of a Mathematical or Physical Character 221 (582–593) (1921) 163–198. doi:10.1098/rsta.1921.0006.

[28] G. R. Irwin, Fracture, Vol. 3 / 6 of Handbuch der Physik / Encyclopedia of Physics, Springer Berlin Heidelberg, Berlin, Heidelberg, 1958, p. 551–590. doi:10.1007/978-3-642-45887-3_5.

[29] Z. Hashin, Finite thermoelastic fracture criterion with application to laminate cracking analysis, Journal of the Mechanics and Physics of Solids 44 (7) (1996) 1129–1145. doi:https://doi.org/10.1016/0022-5096(95)00080-1.

[30] J. Nairn, Fracture mechanics of composites with residual stresses, traction-loaded cracks, and imperfect interfaces, Vol. 27, Elsevier, 2000, p. 111–121. doi:10.1016/S1566-1369(00)80012-6.

[31] D. Taylor, P. Cornetti, N. Pugno, The fracture mechanics of finite crack extension, Engineering Fracture Mechanics 72 (7) (2005) 1021–1038. doi:10.1016/j.engfracmech.2004.07.001.

[32] D. Taylor, The theory of critical distances, Engineering Fracture Mechanics 75 (7) (2008) 1696–1705. doi:https://doi.org/10.1016/j.engfracmech.2007.04.007.

[33] I. Pelekis, L. Susmel, The theory of critical distances to assess failure strength of notched plain concrete under static and dynamic loading, Engineering Failure Analysis 82 (2017) 378–389. doi:https://doi.org/10.1016/j.engfailanal.2017.07.018.

[34] D. Leguillon, Strength or toughness? a criterion for crack onset at a notch, European Journal of Mechanics - A/Solids 21 (1) (2002) 61–72. doi:https://doi.org/10.1016/S0997-7538(01)01184-6.

[35] P. Cornetti, N. Pugno, A. Carpinteri, D. Taylor, Finite fracture mechanics: A coupled stress and energy failure criterion, Engineering Fracture Mechanics 73 (14) (2006) 2021–2033. doi:https://doi.org/10.1016/j.engfracmech.2006.03.010.

[36] T. Methfessel, C. El Yaakoubi-Mesbah, W. Becker, Failure analysis of crack-prone joints with finite fracture mechanics using an advanced modeling approach for the adhesive layer, International Journal of Adhesion and Adhesives 130 (2024) 103608. doi:10.1016/j.ijadhadh.2023.103608.

[37] Z. Yosibash, E. Priel, D. Leguillon, A failure criterion for brittle elastic materials under mixed-mode loading, International Journal of Fracture 141 (1–2) (2006) 291–312. doi:10.1007/s10704-006-0083-6.

[38] I. García, D. Leguillon, Mixed-mode crack initiation at a v-notch in presence of an adhesive joint, International Journal of Solids and Structures 49 (15–16) (2012) 2138–2149. doi:10.1016/j.ijsolstr.2012.04.018.

[39] J. Felger, N. Stein, W. Becker, Mixed-mode fracture in open-hole composite plates of finite-width: An asymptotic coupled stress and energy approach, International Journal of Solids and Structures 122–123 (2017) 14–24. doi:10.1016/j.ijsolstr.2017.05.039.

[40] A. Doitrand, D. Leguillon, G. Molnár, V. Lazarus, Revisiting facet nucleation under mixed mode i + iii loading with t-stress and mode-dependent fracture properties, International Journal of Fracture 242 (1) (2023) 85–106. doi:10.1007/s10704-023-00703-0.

[41] A. Doitrand, A. Sapora, Nonlinear implementation of finite fracture mechanics: A case study on notched brazilian disk samples, International Journal of Non-Linear Mechanics 119 (2020) 103245. doi:10.1016/j.ijnonlinmec.2019.103245.

[42] I. García, B. Carter, A. Ingraffea, V. Mantič, A numerical study of transverse cracking in cross-ply laminates by 3d finite fracture mechanics, Composites Part B: Engineering 95 (2016) 475–487. doi:10.1016/j.compositesb.2016.03.023.

[43] P. Rosendahl, P. Weißgraeber, N. Stein, W. Becker, Asymmetric crack onset at open-holes under tensile and in-plane bending loading, International Journal of Solids and Structures 113-114 (2017) 10–23. doi:https://doi.org/10.1016/j.ijsolstr.2016.09.011.

[44] F. Ferrian, P. Cornetti, A. Sapora, H. Talebi, M. R. Ayatollahi, Crack tip shielding and size effect related to parallel edge cracks under uniaxial tensile loading, International Journal of Fracturedoi:10.1007/s10704-023-00756-1.

[45] A. Sapora, A. Torabi, S. Etesam, P. Cornetti, Finite fracture mechanics crack initiation from a circular hole, Fatigue & Fracture of Engineering Materials & Structures 41 (7) (2018) 1627–1636. doi:https://doi.org/10.1111/ffe.12801.

[46] A. Doitrand, D. Leguillon, Asymptotic analysis of pore crack initiation near a free edge, Theoretical and Applied Fracture Mechanics 116 (2021) 103125. doi:https://doi.org/10.1016/j.tafmec.2021.103125.

[47] P. Weißgraeber, D. Leguillon, W. Becker, A review of finite fracture mechanics: crack initiation at singular and non-singular stress raisers, Archive of Applied Mechanics 86 (1) (2016) 375–401. doi:https://doi.org/10.1007/s00419-015-1091-7.

[48] A. Doitrand, T. Duminy, H. Girard, X. Chen, A review of the coupled criterion, working paper or preprint (Mar 2023).

[49] T. Laschuetza, T. Seelig, Remarks on dynamic cohesive fracture under static pre-stress — with a comparison to finite fracture mechanics, Engineering Fracture Mechanics 242 (2021) 107466. doi:https://doi.org/10.1016/j.engfracmech.2020.107466.

[50] J. Le Pavic, T. Bonnemains, É. Lolive, G. Stamoulis, D. Da Silva, D. Thévenet, Failure load prediction of a tubular bonded structures using a coupled criterion, Theoretical and Applied Fracture Mechanics 108 (2020) 102531. doi:https://doi.org/10.1016/j.tafmec.2020.102531.

[51] A. Chao Correas, P. Cornetti, M. Corrado, A. Sapora, Finite fracture mechanics extension to dynamic loading scenarios, International Journal of Fracture 239 (2022) 149–165. doi:https://10.1007/s10704-022-00655-x.

[52] A. Doitrand, G. Molnár, D. Leguillon, E. Martin, N. Carrère, Dynamic crack initiation assessment with the coupled criterion, European Journal of Mechanics-A/Solids 93 (2022) 104483. doi:https://doi.org/10.1016/j.euromechsol.2021.104483.

[53] X. Chen, A. Doitrand, N. Godin, C. Fusco, Crack initiation in PMMA plates with circular holes considering kinetic energy and nonlinear elastic material behavior, Theoretical and Applied Fracture Mechanics 124 (2023) 103783. doi:https://doi.org/10.1016/j.tafmec.2023.103783.

[54] A. Leite, V. Mantič, F. París, Crack onset in stretched open hole PMMA plates considering linear and nonlinear elastic behaviours, Theoretical and Applied Fracture Mechanics 114 (2021) 102931. doi:https://doi.org/10.1016/j.tafmec.2021.102931.

[55] G. Marshall, L. H. Coutts, J. Williams, Temperature effects in the fracture of pmma, Journal of Materials Science 9 (1974) 1409–1419.

[56] P. W. Beaumont, R. J. Young, Failure of brittle polymers by slow crack growth: Part 1 crack propagation in polymethylmethacrylate and time-to-failure predictions, Journal of materials science 10 (1975) 1334–1342.

[57] O. Miller, L. Freund, A. Needleman, Energy dissipation in dynamic fracture of brittle materials, Modelling and Simulation in Materials Science and Engineering 7 (4) (1999) 573.

[58] J. Scheibert, C. Guerra, F. Célarié, D. Dalmas, D. Bonamy, Brittle-quasibrittle transition in dynamic fracture: An energetic signature, Physical Review Letters 104 (4) (2010) 045501.

[59] R. Heinzmann, R. Seghir, S. Y. Alam, J. Réthoré, Experimental investigation of the alternate recurrence of quasi-static and dynamic crack propagation in pmma, International Journal of Fracture 242 (2) (2023) 227–245.

[60] Q.-Z. Wang, L. Xing, Determination of fracture toughness kic by using the flattened brazilian disk specimen for rocks, Engineering Fracture Mechanics 64 (2) (1999) 193–201. doi:https://doi.org/10.1016/S0013-7944(99)00065-X.

[61] S. Wu, J. Ma, Y. Cheng, M. Xu, X. Huang, Numerical analysis of the flattened brazilian test: Failure process, recommended geometric parameters and loading conditions, Engineering Fracture Mechanics 204 (2018) 288–305. doi:https://doi.org/10.1016/j.engfracmech.2018.09.024.

[62] A. Doitrand, R. Estevez, D. Leguillon, Comparison between cohesive zone and coupled criterion modeling of crack initiation in rhombus hole specimens under quasi-static compression, Theoretical and Applied Fracture Mechanics 99 (2019) 51–59. doi:https://10.1016/j.tafmec.2018.11.007.

[63] B. Croquelois, Comportement à rupture des matériaux hétérogènes fragiles : application au comprimé pharmaceutique, These de doctorat, Bordeaux (dec 2020).